Hindawi
Discrete Dynamics in Nature and Society
Volume 2024, Article ID 9763528, 1 page
https://doi.org/10.1155/2024/9763528

Retraction

Retracted: Hysteretic Energy Demand under Superposition of Bidirectional Ground Motions

Discrete Dynamics in Nature and Society

Received 23 January 2024; Accepted 23 January 2024; Published 24 January 2024

This article has been retracted by Hindawi following an investigation undertaken by the publisher [1]. This investigation has uncovered evidence of one or more of the following indicators of systematic manipulation of the publication process:

(1) Discrepancies in scope

(2) Discrepancies in the description of the research reported

(3) Discrepancies between the availability of data and the research described

(4) Inappropriate citations

(5) Incoherent, meaningless and/or irrelevant content included in the article

(6) Manipulated or compromised peer review

The presence of these indicators undermines our confidence in the integrity of the article's content and we cannot, therefore, vouch for its reliability. Please note that this notice is intended solely to alert readers that the content of this article is unreliable. We have not investigated whether authors were aware of or involved in the systematic manipulation of the publication process.

Wiley and Hindawi regrets that the usual quality checks did not identify these issues before publication and have since put additional measures in place to safeguard research integrity.

We wish to credit our own Research Integrity and Research Publishing teams and anonymous and named external researchers and research integrity experts for contributing to this investigation.

The corresponding author, as the representative of all authors, has been given the opportunity to register their agreement or disagreement to this retraction. We have kept a record of any response received.

References

[1] F. Wang, J. Shi, and P. Chen, "Hysteretic Energy Demand under Superposition of Bidirectional Ground Motions," *Discrete Dynamics in Nature and Society*, vol. 2021, Article ID 4623414, 13 pages, 2021.

Hindawi
Discrete Dynamics in Nature and Society
Volume 2021, Article ID 4623414, 13 pages
https://doi.org/10.1155/2021/4623414

Research Article

Hysteretic Energy Demand under Superposition of Bidirectional Ground Motions

Feng Wang, Jialin Shi, and Pengyan Chen

College of Civil Engineering, Dalian Minzu University, Dalian 116650, Liaoning, China

Correspondence should be addressed to Feng Wang; wfeng@dlnu.edu.cn

Received 27 July 2021; Revised 26 September 2021; Accepted 19 October 2021; Published 8 December 2021

Academic Editor: Ahmed Farouk

To address the irrationality of making a structure subjected to bidirectional ground motions equivalent to an SDOF system, a new approach method is presented in this paper. The ratio between modal participation factors of the two components of the structure is expressed as γ, and the superposition of bidirectional ground motions is regarded as one-directional earthquake excitation for the equivalent SDOF system. Based on this, an energy balance equation is established, and a method used to estimate normalized hysteretic energy (NHE) is proposed. Analysis of the ratio between NHE ($\gamma \neq 0$) and NHE ($\gamma = 0$) is suggested in order to analyze the influence of bidirectional ground motions on hysteretic energy demand, and then, "α_1 = NHE ($\gamma \neq 0$)/NHE ($\gamma = 0$)" is defined, and bidirectional ground motion records for different soil sites are selected for establishing superimposed excitations. In addition, the period range of 0–5 s for the energy spectrum is divided into 6 ranges. In each period range, the means of α_1 are defined as α. The curves of α of constant ductility factors for different soil sites are established, in which α is the vertical coordinate and γ is the horizontal coordinate. Through nonlinear response history analysis, the influence of soil types at different sites, the ductility factor, the ratio of modal participation factors, and the period on the values of α are analyzed. According to the analytical results, correction coefficient α_s (the simplified value of α) is obtained so that the hysteretic energy demand under bidirectional ground motions can be determined.

1. Introduction

Proper design of earthquake-resistant structures is extremely important for seismically active areas because it can be a key instrument that shapes economic and social opportunities. However, designing safe and economically viable structures is a very complex and multidisciplinary process that requires knowledge of a large number of engineering tools, parameters, and skills. Response spectra are also used as a basis for determining artificial earthquake records (e.g., [1, 2]). Response spectra have been recorded in practice since the 1971 San Fernando earthquake [3, 4], are now considered a basic tool for determining cutting forces and dimensioning structures, and are also used in preliminary calculations of important structures [3, 5]. The reason for the good acceptance and frequent application of the response spectrum lies in the simplicity of application, very low requirements for computer resources, and reasonable results for dimensioning structures. Response spectra contain information on the intensity and frequency composition of earthquakes, and their application takes into account the dynamic nature of the problem in structural calculations. However, calculation methods using the response spectrum are primarily applicable and give reasonable results for structures with a pronounced influence of lower forms of oscillation (e.g., [3, 6]). Furthermore, it is common knowledge that normalized response spectra are fabricated using single-degree systems embedded in a rigid substrate (e.g., [7, 8]).

Over the years, energy-based seismic design (EBSD) has been widely developed. Benavent-Climent [9] and Ghodrati Amiri et al. [10] provided an EBSD process for restructuring already built-in structures. Habibi et al. [11] proposed an EBSD process for rearranging structures with passive energy dissipation systems. Wang et al. [12] proposed an earthquake-induced story to estimate hysteretic energy (HE) according to the energy relationship between the SDOF and the original system. Some researchers (Zhang et al. [13] and Greco et al. [14]) use the well-known Park–Ang model to

estimate the damage level of structures in which the HE is an important index. The energy requirement is an important indicator for assessing seismic induction and seismic capabilities [15, 16].

To determine the dissipated earthquake energy of a structure from an energy spectrum, the structure itself should first be made equivalent to an SDOF system, and then, the energy demand of this equivalent SDOF system can be obtained via the energy spectrum to further compute the dissipated earthquake energy of the structure (Bruneau and Wang [17], Decanini and Mollaioli [18], and Erduran [19]). Currently, various energy spectra for the SDOF system have been developed, such as earthquake input energy spectrum [20], hysteretic energy spectrum [21, 22], absorbed energy spectrum [23], momentary energy spectrum [24], and inelastic cyclic demand spectrum [25]. However, for a structure subject to multidimensional ground motions (GMs), rational analysis shows that instead of one-component GM, it is the superposition of multicomponent GMs combined through modal participation factors that affect the results of responses of the analyzed structure. This is inconsistent with the traditional energy spectrum. Wang and Li [26] proposed a method to solve this problem, in which a structure under bidirectional GMs was made equivalent to a single-mass system with two degrees of freedom, and the HE and earthquake input energy spectra were established based on this equivalent system; however, further research studies about the energy relationship between this equivalent system and the structure were required for application of this theory. Reyes and Chopra [27] suggested a procedure to estimate structural responses under bidirectional GMs, in which the structural responses were calculated in two orthogonal directions, and the complete quadratic combination (CQC) rule was applied to combine the responses of these two components. This method is easy to use; however, it does not take into account the bidirectional coupling of nonlinear responses of structures. In this paper, a novel approach is proposed, in which the superposition of bidirectional GMs is applied as one-directional excitations of the equivalent SDOF systems, and then used to analyze the HE demand of structures.

2. Principle

2.1. Energy Equation of Modal Equivalent SDOF Systems. Consider an n-story building. The equation of motion governing the response of the n-story building subjected to bidirectional GMs (BGMs) (along x and y components) is expressed as

$$\mathbf{M}\ddot{\mathbf{u}}\,(t) + \mathbf{C}\dot{\mathbf{u}}(t) + \mathbf{F}(t) = -\mathbf{M}\boldsymbol{\iota}_x\ddot{\mathbf{u}}_{gx}\,(t) - \mathbf{M}\boldsymbol{\iota}_y\ddot{\mathbf{u}}_{gy}(t), \tag{1}$$

where $\mathbf{M}$ and $\mathbf{C}$ are the diagonal mass and damping matrices and $\mathbf{F}(t)$ and $\mathbf{u}(t)$ are the resisting forces and displacement response vector, given as $[\mathbf{u}_x\ \mathbf{u}_y\ \mathbf{u}_\theta\ ]^T$ in which $\mathbf{u}$ denotes the x, y, and torsion-directional displacement subvector, respectively. The energy balance equation of the building from equation (1) can be

$$\int_0^{t_0} d\mathbf{u}\,(t)^T\mathbf{M}\ddot{\mathbf{u}}\,(t) + \int_0^{t_0} d\mathbf{u}\,(t)^T\mathbf{C}\dot{\mathbf{u}}(t) + \int_0^{t_0} d\mathbf{u}\,(t)^T\mathbf{F}(t) = -\int_0^{t_0} d\mathbf{u}\,(t)^T\left(\mathbf{M}\boldsymbol{\iota}_x\ddot{u}_{gx}(t) + \mathbf{M}\boldsymbol{\iota}_y\ddot{u}_{gy}(t)\right). \tag{2}$$

Here, $t_0 \in [0\ t_1]$, where t_1 is the duration of GM, and $d\,\mathbf{u}(t)$ equals to $\dot{\mathbf{u}}\,(t)\mathrm{d}t$, where $\dot{\mathbf{u}}\,(t)$ is the velocity vector. The energy terms from left to right of this equation are kinetic energy $E_k(t)$, viscous damping energy $E_d(t)$, HE $E_h(t)$, and input energy $E_I(t)$, respectively, of the considered building. According to the hypothesis of an equivalent SDOF system, $\mathbf{u}(t)$ for an inelastic system can be expanded based on the natural vibration patterns of the corresponding linear elastic system:

$$\mathbf{u}(t) \approx \sum_{i=1}^{3n} \boldsymbol{\varphi}_i q_i(t), \tag{3}$$

where $\boldsymbol{\varphi}_i$ is the ith mode shape vector which includes three subvectors $\boldsymbol{\varphi}_{xi}$, $\boldsymbol{\varphi}_{yi}$, and $\boldsymbol{\varphi}_{\theta i}$. Equation (3) is substituted into Equation (2); by premultiplying both sides by $\boldsymbol{\varphi}_{iT}$,

$$\begin{aligned}&\int_0^{t_0} \boldsymbol{\varphi}_i^T\mathbf{M}\boldsymbol{\varphi}_i\ddot{q}_i\,(t)\dot{q}_i(t)\mathrm{d}t + \int_0^{t_0} \boldsymbol{\varphi}_i^T\mathbf{C}\boldsymbol{\varphi}_i\dot{q}_i(t)\dot{q}_i(t)\mathrm{d}t + \int_0^{t_0} F_i(t)\dot{q}_i(t)\mathrm{d}t \\ &= -\int_0^{t_0} \boldsymbol{\varphi}_i^T\mathbf{M}\boldsymbol{\varphi}_i\left(\Gamma_{xi}\ddot{\mathbf{u}}_{gx}(t) + \Gamma_{yi}\ddot{\mathbf{u}}_{gy}(t)\right)\dot{q}_i(t)\mathrm{d}t, \quad (i = 1, \ldots, 3n),\end{aligned} \tag{4}$$

where Γ_{xi} and Γ_{yi} are modal participation factors along x and y components, respectively. The ith modal resisting force $F_i(t)$ can be denoted as $\boldsymbol{\varphi}_i{}^T\mathbf{K}_{ep}(t)\boldsymbol{\varphi}_i q_i(t)$, where $\mathbf{K}_{ep}(t)$ is the elastic-plastic stiffness matrices (instantaneous).

In previous research studies, the following process is commonly used. Firstly, the 1st modal structure is simplified as two 2D models along x and y directions, respectively, and the responses, Q_{xi} and Q_{yi}, are solved, respectively, through nonlinear response history analysis. After that, Q_{xi} and Q_{yi} are brought into the SRSS rule, and the 1st modal responses can be determined. The above procedure is repeated for different modes. Finally, the CQC rule is used for calculating

the structural responses based on multimodal responses. In this paper, a new idea is proposed to solve structural responses under BGMs.

$$\int_0^{t_0} \boldsymbol{\varphi}_i^T \mathbf{M} \boldsymbol{\varphi}_i \ddot{q}_i(t) \dot{q}_i(t) \mathrm{d}t + \int_0^{t_0} \boldsymbol{\varphi}_i^T \mathbf{C} \boldsymbol{\varphi}_i \dot{q}_i(t) \dot{q}_i(t) \mathrm{d}t + \int_0^{t_0} F_i(t) \dot{q}_i(t) \mathrm{d}t = -\int_0^{t_0} \boldsymbol{\varphi}_i^T \mathbf{M} \boldsymbol{\varphi}_i \Gamma_i U_{gi}(t) \dot{q}_i(t) \mathrm{d}t, \quad (i = 1, \ldots, 3n). \tag{5}$$

Here, $\ddot{U}_{gi}(t)$ is superimposed ground acceleration (A), and $\ddot{U}_{gi}(t) = \ddot{u}_{gx}(t) + \gamma_i \ddot{u}_{gy}(t)$, in which $\gamma_i = \Gamma_{yi}/\Gamma_{xi}$, and its range is from -1 to 1. The $\ddot{U}_{gi}(t)$ can be considered as an earthquake excitation.

For the case of $|\Gamma_{xi}| \le |\Gamma_{yi}|$, we set $\Gamma_{yi} = \Gamma_i$, and the superimposed ground "A" is replaced with $\ddot{U}_{gi}(t) = \gamma_i \ddot{u}_{gx}(t) + \ddot{u}_{gy}(t)$, in which $\gamma_i = \Gamma_{xi}/\Gamma_{yi}$. The above relationship can be expressed as

$$\begin{aligned} &\text{For } |\Gamma_x| \ge |\Gamma_y|, \ddot{U}_g(t) = \ddot{u}_{gx}(t) + \gamma \ddot{u}_{gy}(t), \quad \text{where } \gamma = \frac{\Gamma_y}{\Gamma_x}, \\ &\text{For } |\Gamma_y| \ge |\Gamma_x|, \ddot{U}_g(t) = \gamma \ddot{u}_{gx}(t) + \ddot{u}_{gy}(t), \quad \text{where } \gamma = \frac{\Gamma_x}{\Gamma_y}. \end{aligned} \tag{6}$$

For the case of $|\Gamma_{xi}| \ge |\Gamma_{yi}|$, set $\Gamma_{xi} = \Gamma_i$, and then, Equation (4) can be rewritten as

Here, when $\gamma = 0$ and $\ddot{U}_g(t) = \ddot{u}_{gx}(t)$ (or $\ddot{u}_{gy}(t)$), it is one-directional ground "A," and when $\gamma \ne 0$, $\ddot{U}_g(t)$ is superimposed "A" of BGMs. The transformational relation is illustrated in Figure 1, in which the two-component ground "A"s of Taft are superimposed as a one-component "A" with the ratio $\gamma = 6$.

Defining $q_i(t) = d_i(t) \bullet \Gamma_i$, substituting it into Equation (5), and after predividing by $\boldsymbol{\varphi}_i{}^T \mathbf{M} \boldsymbol{\varphi}_i$,

$$\int_0^{t_0} d_i(t) \dot{d}_i(t) \mathrm{d}t + 2\xi\omega_i \int_0^{t_0} \dot{d}_i(t) \dot{d}_i(t) \mathrm{d}t + \int_0^{t_0} f_i(t) \dot{d}_i(t) \mathrm{d}t = -\int_0^{t_0} \ddot{U}_{gi}(t) \dot{d}_i(t) \mathrm{d}t, \quad (i = 1, \ldots, 3n). \tag{7}$$

Here, $f_i(t) = F_i(t)/\boldsymbol{\varphi}_i{}^T \mathbf{M} \boldsymbol{\varphi}_i \Gamma_i$, ξ is damping ratio, and ω_i is natural frequency of ith mode of structure. Equation (7) can be regarded as the energy balance equations of $3n$ independent modal equivalent SDOF systems with mass equals to 1. The energy terms from left to right of Equation(7) are kinetic energy $e_{k,i}(t_0)$, viscous damping energy $e_{d,i}(t_0)$, HE $e_{h,i}(t_0)$, and input energy $e_{I,i}(t_0)$, respectively, of the ith modal equivalent SDOF system.

By the above derivation, structural HE due to earthquake can be determined through the following equation:

$$E_h(t_0) \approx \sum_{i=1}^{3n} \boldsymbol{\varphi}_i^T \mathbf{M} \boldsymbol{\varphi}_i \Gamma_i^2 \cdot e_{h,i}(t_0). \tag{8}$$

The relation of deformation and energy dissipation between a structure and its modal equivalent SDOF systems is illustrated in Figure 2, in which the structure subjected to bidirectional GMs and each equivalent SDOF system is subject to their superposition, and the ratio γ in superposition equation depends on the modal participation factors of the structure.

Considering the variation of mode shape in plastic response range of structures, the elastic mode shapes in Equation (8) can be substituted by elastic-plastic mode shapes, which can be obtained by pushover analysis or modal pushover analysis [28, 29].

2.2. Energy Demands under Superposition of Bidirectional Ground Motions. A modal equivalent SDOF system mentioned above is considered. The instantaneous relative displacement is defined as $\mu(t)$, and $\mu(t) = d(t)/d_{yie}$, where d_{yie} is yield displacement. The maximum value of $\mu(t)$ equals to ductility factor μ. Substituting μ (t) into Equation (7), the following equation can be derived:

$$d_{yie}^2 \int_0^{t_0} \ddot{\mu}(t) \dot{\mu}(t) \mathrm{d}t + 2\xi\omega d_{yie}^2 \int_0^{t_0} \dot{\mu}(t) \dot{\mu}(t) \mathrm{d}t + \omega^2 d_{yie}^2 \int_0^{t_0} \frac{f(t)}{f_{yie}} \dot{\mu}(t) \mathrm{d}t = -d_{yie} \int_0^{t_0} \ddot{U}_g(t) \dot{\mu}(t) \mathrm{d}t, \tag{9}$$

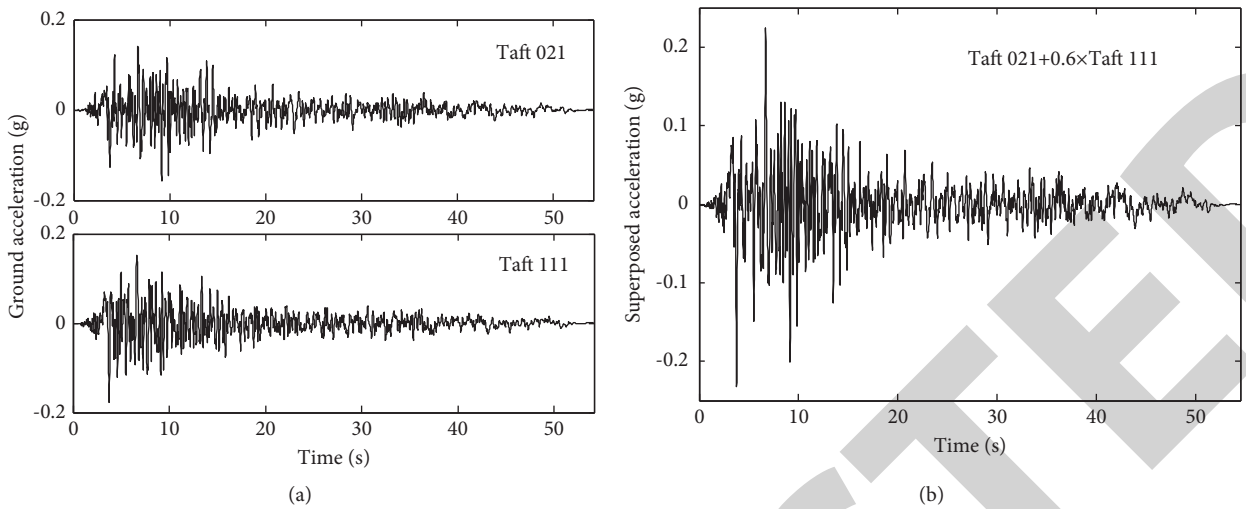

Figure 1: The superposition of bidirectional ground "A" records of Taft. (a) Bidirectional ground "A"s. (b) Superposition of bidirectional "A."

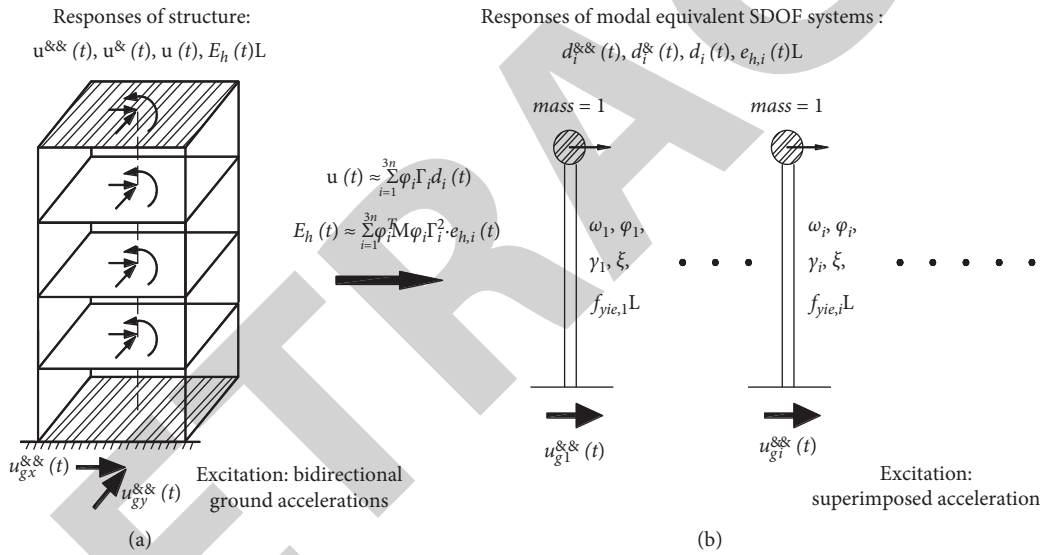

Figure 2: The relation between (a) structure and (b) modal equivalent SDOF systems.

where f_{yie} is the yield force of the equivalent SDOF system. The mass of the SDOF system equals to 1; therefore, $f_{yie} = \omega^2 d_{yie}$, and the peak force in the linear elastic stage can be $\max|f_e(t)| = \beta \cdot \mathrm{PSA}$, where β is amplification coefficient spectrum under superposition of BGMs and PSA is the abbreviation of peak superimposed "A" and $\mathrm{PSA} = \max(|\ddot{U}_g(t)|)$. The strength reduction factors can be expressed as $R = \max|f_e(t)|/f_{yie}$. According to the above expression, d_{yie} is expressed as

$$d_{yie} = \frac{\beta \cdot \mathrm{PSA}}{\omega^2 \cdot R}. \tag{10}$$

Substituting Equation (10) into (9), the energy equation can be rewritten as

$$\frac{\beta^2 \mathrm{PSA}^2}{\omega^4 R^2} \int_0^{t_0} \ddot{\mu}(t)\dot{\mu}(t)\mathrm{d}t + \frac{2\xi\beta^2 \mathrm{PSA}^2}{\omega^3 R^2} \int_0^{t_0} \dot{\mu}(t)\dot{\mu}(t)\mathrm{d}t + \frac{\beta^2 \mathrm{PSA}^2}{\omega^2 R^2} \int_0^{t_0} \frac{f(t)}{f_{yie}}\dot{\mu}(t)\mathrm{d}t = -\frac{\beta \cdot \mathrm{PSA}}{\omega^2 R} \int_0^{t_0} \ddot{U}_g(t)\dot{\mu}(t)\mathrm{d}t. \tag{11}$$

According to the process of derivation from Equations (7) to (11), the energy terms from left to right of Equation (11) are still kinetic energy $e_{k,i}(t_0)$, viscous damping energy $e_{d,i}(t_0)$, HE $e_{h,i}(t_0)$, and input energy $e_{I,i}(t_0)$, respectively.

The PSA of each pair of GMs are different, so, in order to make mean energy demand which is not affected by PSA, both sides of Equation (11) are divided by PSA squared, and the energy equation is rewritten as

$$\frac{\beta^2}{\omega^4 R^2}\int_0^{t_0}\ddot{\mu}(t)\dot{\mu}(t)\mathrm{d}t+\frac{2\xi\beta^2}{\omega^3 R^2}\int_0^{t_0}\dot{\mu}(t)\dot{\mu}(t)\mathrm{d}t+\frac{\beta^2}{\omega^2 R^2}\int_0^{t_0}\frac{f(t)}{f_{yie}}\dot{\mu}(t)\mathrm{d}t=-\frac{\beta}{\omega^2 R}\int_0^{t_0}\frac{\ddot{U}_g(t)}{\mathrm{PSA}}\dot{\mu}(t)\mathrm{d}t. \tag{12}$$

Here, $\ddot{U}_g(t)/\mathrm{PSA}$ is normalized superimposed "A," and each normalized energy term in the equation is the ratio of energy to PSA squared. The 3rd term on the left side of Equation (12) is the normalized HE (NHE).

2.3. Normalized Hysteretic Energy Spectrum under Superposition of Bidirectional Ground Motions. The procedure for establishing NHE spectrum under superposition of BGMs is as follows:

(1) The ratio γ between bidirectional modal participation factors is given, and then, the superimposed "A" time history $\ddot{U}_g(t)$ of the SDOF system is determined using Equation (6).

(2) The damping ratio ξ is given, and a specific period T is selected to calculate the corresponding amplification factor spectrum β, where the relationship between the period and frequency is $T=2\pi/\omega$.

(3) The ductility factor μ_o of a target is chosen.

(4) The parameter R is set to a value smaller than μ_o, and it is substituted into Equation (12) to calculate the maximum relative displacement $\max|\mu(t)|$.

(5) Assume $\Delta=|\mu_o-\max|\mu(t)||$ if Δ is within an acceptable range; namely, if $\max|\mu(t)|$ is close enough to μ_o, then pause calculation and determine the NHE demand using Equation (13). Otherwise, continue calculation to the next step:

$$\begin{cases}\mathrm{NHE}(\gamma,\mu,R,T,\xi)=\dfrac{T^2\beta^2}{4\pi^2R^2}\displaystyle\int_0^{t_1}\frac{f(t)}{f_{yie}}\dot{\mu}(t)\mathrm{d}t,\\ \text{s.t.}\quad \text{Equation (12)};\quad \mu=\max|\mu(t)|,\end{cases} \tag{13}$$

where the instantaneous relative displacement $\mu(t)$ is obtained by solving Equation (12) and t_1 is the duration of the bidirectional GMs.

(6) Properly raise the value of R. For example, $R=R+0.1$, and then, repeat Steps 4–5 until the requirement of "$\max|\mu(t)|\approx\mu_o$" is satisfied. After that, determine NHE demand using Equation (13).

(7) Apply a different period T (e.g., $T=0$–5 s), and then, repeat Steps 2–6 to establish the NHE spectra corresponding to a given γ.

3. Selection of Earthquake Records

For analyzing the mean HE demand, 89 pair horizontal BGM records for hard soil site (HSS) ($V_s=360$–750 m/s), ISS (intermediate hard (soft) soil site) ($V_s=180$–360 m/s), and SSS (soft soil site) ($V_s<180$ m/s), corresponding to B, C, and D, respectively, for USGS, are selected (Tables 1–3). The conditions for choosing these records are (1) magnitude equal to 6 to 8, (2) fault distance equal to 15 km to 45 km, (3) and peak "A" for x or y directions are greater than or equal to 0.1 g, approximately.

The amplification coefficient spectra $\beta(T,\xi)$ is illustrated in Figure 3 for three sites with different types of soils based on the original one-directional earthquake "A" records (traditional spectrum, and $\gamma=0$) and superposition of bidirectional earthquake "A" records (proposed in this paper, and $\gamma\neq0$). For the latter case, γ is set as 1 and -1 in this figure, respectively. For this reason, the two ratios of modal participation factors may result in a larger deviation of results. As shown in Figure 3, the spectra of superimposed GMs are much closed to the spectra of one-directional GMs, which indicates that the superimposed earthquake "A"s still have the typical characteristics of the different soil sites.

4. Analysis of Hysteretic Energy Demand

4.1. Analysis of NHE Spectra. According to Equations (5)–(7), NHE($\gamma=0$) is the normalized HE under one-directional GM, and NHE($\gamma\neq0$) is the normalized HE under the superposition of bidirectional GMs. Figure 4 displays the mean spectra of NHE ($\gamma=0$) for soil types at different sites. As shown in this figure, the spectrum for each soil base has its own spectral shape features. The spectral curves of the 3 soil bases are all made upward, peak platform, and downward levels, and the time limits for each phase are obviously affected by the ductility factor and the soil type.

Figure 5 illustrates the comparison of NHE spectra between one-directional GMs and superposition of bidirectional GMs ($\gamma=0.8$ and -0.8). As shown in this figure, the difference between $\gamma=0$ and $\gamma\neq0$ is obvious, and it may be affected by soil type, period, ductility factor, positive and negative of γ, and value of γ. In this figure, γ is only set as 0.8 and -0.8, but for the other values of γ, the system analyses are as follows.

4.2. Analysis of α Curves. The mean demand of NHE ($\gamma\neq0$) is influenced by some parameters. Many researchers have studied the HE spectrum under one-directional GM and achieved various results. In the interest of simplification, the ratios between NHE ($\gamma\neq0$) and NHE ($\gamma=0$) are analyzed in this paper to study the HE demand under the superposition of bidirectional GMs. An approach is used to establish the ratio of NHE ($\gamma\neq0$)/NHE ($\gamma=0$) according to soil types at

Table 1: The ground "A" records for HSS (34 pairs).

Stations	Earthquakes	Components	Stations	Earthquakes	Components
1095 Tafe Lin-Coln School	Kern Country (52/7/21,M7.4)	TAF021	6604 Cerro Prieto	Victoria, Mexico (80/06/09,Ms6.4)	CPE045
		TAF111			CPE315
1652Amderson-Dam	Lorna Prieta (89/10/18,M69)	AND270	89324 Rio Dell Overpass-FF	Cape Mendocina (92/04/25,M7.1)	RIO270
		AND360			RIO360
24157 LA-Baldwin Hills	Northridge (94/1/17,M6.7)	BLD090	CHY029	Chi-Chi (99/09/20,M7.6)	CHY029_N
		BlD360			CHY029_W
14403 LA-116th st School	Northridge (94/01/17,M6.7)	116090	ALS	Chi-Chi (99/09/20,M7.6)	ALS-E
		116360			ALS-N
24605LA-Univ.Hospital	Northridge (94/01/17,M6.7)	UNI005	CHY052	Chi-Chi (99/09/20,M7.6)	CHY029_E
23 Coolwater	Landers (92/06/28,7.3)	UNI095 CLW-LN CLW-TR	1061 Lamont	Duzce (99/11/12,M7.1)	CHY029_N 1061-N 1061-E
6604 Cerro Prieta	Imperial Valley (79/10/15,M6.5)	H-CPE147	Arcelik	Kocaeli (99/08/17,M7.4)	ARC000
		H-CPE237			ARC090
57504 Coyote Lake Dam	Loma Prieta (89/10/18,M6.9)	CLD195	24577 Fort Irwin	Landers (92/06/28,M7.3)	FTI000
		CLD285			FTI090
Tcu045	Chi-Chi (99/0920,M7.6)	TCU045-N	57064 Fremont-Misssion Sen Jose	Loma Prieta (89/10/18,M6.9)	FRE000
		TCU045-W			FRE090
Tcu047	Chi-Chi (99/0920,M7.6)	TCU045-N	57383 Gilroy ArrayW#6	Loma Prieta (89/10/18,M6.9)	G06000
		TCU045-W			G06090
90021LA-N Westmoreland	Northridge (94/01/17,M6.7)	WST000	58378 APEEL7_pulgas	Loma Prieta (89/10/18,M6.9)	A07000
		WST270			A07000
CHY086	Chi-Chi (99/09/20,M6.7)	CHY086-N	58498 Hayward-BART Sta	Loma Prieta (89/10/18,M6.9)	HWB220
		CHY086-W			HWB310
286 Superstition Mtn Camera	Imperial Valley (79/10/15,M6.5)	H.SUP045	47006 Gilory Gavialn Coll	Morgan Hill (84/04/24,M6.2)	GIL067
		H.SUp135			GIL337
12149 Desert Hot Springs	Landers (92/06/28,M7.3)	DSP000	24607 Laka Hughes#12A	Northridge (94/01/17,M6.7)	H12090
		DSP090			H12180
24389LA-Century City CC North	Northridge (94/01/17,M6.7)	CCN090	24611 LA-Temple Hope	Northridge (94/01/17,M6.7)	TEM090
		CCN360			TEM180
14403 LA-116thst School	Whittier Narrows (87/10/01,M6.0)	A-116270	90020 LA-W15 *St	Northridge (94/01/17,M6.7)	W15090
		A-116360			W15180
90009 N Hollywood Coldwater	Whittier Narrows (87/10/01,M6.0)	A-CWC180	900333_LA Cyper Ava	Northridge (94/01/17,M6.7)	CYP053
		A-CWC270		Northridge (94/01/17,M6.7)	CYP143

different sites, the influence of the soil type, the ductility factor μ, and the ratio between modal participation factors of two components, γ, are analyzed, and the approximate relationships concerning NHE ($\gamma \neq 0$)/NHE ($\gamma = 0$) are provided. In addition, the damping ratio ξ is set as 0.05; according to the process mentioned above, NHE demand can be solved.

According to the range of γ, the typical values of γ are selected as −1.0, −0.8, −0.6, −0.4, −0.2, 0, 0.2, 0.4, 0.6, 0.8, and 1.0. The period T is divided into 6-period ranges: 0.5–1 s, 1–2 s, 2–3 s, 3–4 s, and 4–5 s. α_1 is defined as the ratio between NHE ($\gamma \neq 0$) and NHE ($\gamma = 0$), and for the convenience of analysis, α is defined as the mean of α_1 for each period range. Given γ as horizontal coordinate and α as vertical

Table 2: The ground "A" records for ISS (35 pairs).

Stations	Earthquakes	Components	Stations	Earthquakes	Components
6621 Chihuahua	Imperial Valley (79/10/15, M6.5)	CHI012	NST	Chi-Chi (99/09/20,M7.6)	NST-E
		CHI282			NST-N
1695 Sunnyvale Colton Ava	Loma Prieta (89/10/18,M6.9)	SVL270	6622 Compuertas	Imperial Valley (79/10/15,M6.5)	H-CMP015
		SVL360			H-CMP285
1028 Holister City Hall	Loma Prieta (89/10/18,M6.9)	HCH090	36227 Parkfield Cholame 5W	Coalinga (89/05/02,M6.4)	H-C05270
		HCH180			H-C05360
22074 Yermo Fire Station	Landers (92/06/28,M7.3)	YER270	Iznik	Kocaeli (99/08/17,M7.4)	IZN180
		YER360			IZN090
90063 Glendale Las Palmas	Northridge (94/01/17,M6.7)	GLP177	57066AgnewState Hospital	Loma Prieta (89/10/18,M6.9)	AGW000
		GLP267			AGW090
90016 LA-N Faring RD	Northridge (94/01/17).M6.7)	FAR000	57425 Gilroy Array#7	Loma Prieta (89/10/18,M6.9)	GMR000
		FAR090			GMR090
90091 LA-Saturn St	Northridge (94/01/17).M6.7	STN020	47125 Capitola	Morgan Hill (84/04/24,M6.2)	CAP042
		STN110			CAP132
TCU 042	Chi-Chi (99/09/20,M7.6)	TCU042-N	47380 Gilroy Array #2	Morgan Hill (84/04/24,M6.2)	G02000
		TCU042-W			G02090
TCU107	Chi-Chi (99/09/20,M7.6)	TCU0107-N	24303 LA-Hollywood Stor	Northridge (94/01/17,M6.7)	HOL090
		TCU107-N			HOL360
CHY036	Chi-Chi (99/0920,M7.6)	CHY036-N	24309 Leona Valley#6	Northridge (94/01/17,M6.7)	LV6090
		CHY036-N			LV6360
6605 Delta	Imperial Valley (79/10/15,M6.5)	H-DLT262	90034 LA-Fletcher DR	Northridge (94/01/17,M6.7)	FLE144
		H-DLT352			FLE234
CHY010	Chi-Chi (99/0920,M7.6)	CHY010-E	90054 LA Centinela ST	Northridge (94/01/17,M6.7)	CEN155
		CHY010-N			CEN245
CHY034	Chi-Chi (99/0920,M7.6)	CHY034-E	12025 Palm Springs Airport	N Palm Springs (86/07/08,M6.0)	PSA000
		CHY034-N			PSA090
CHY046	Chi-Chi (99/0920,M7.6)	CHY046-N	994 Gormon Oso Pump Plant	San Fernando (71/02/09,M6.6)	OPP000
		CHY046-W			OPP270
Atakoy	Kocaeli (99/08/17,M7.4)	ATK000	135 LA-Hollywood Stor Lot	San Fernando (71/02/09,M6.6)	PEL090
		ATK090			PEL090
Bolu	Duzca (99/11/12M7.1)	BOL000	6621 Chihuahua	Victoria (80/06/09,M6.4)	CHI102
		BOL090			CHI192
EI Centro Array #1	Imperial Valley (79/10/15,M6.5)	H-E01140	90003Northridge Saticoy St	Whittier Narrows (87/10/01,M6.0)	A-STC090
		H-E01230			A-STC180
5061 Calipatria Fire State	Imperial Valley (79/10/15,M6.5)	H-CAL225			
		H-CAL315			

coordinate, and then, α curves of constant ductility factors can be established (see Figures 6–8).

Figure 6 displays the curves of α of constant ductility factors for hard soil site. From this figure, the following are clear. (1) During the period range of 0–2 s, with the increase of γ, α shows a tendency to decrease; for the case that the ductility factor is smaller and period is longer, this decreasing tendency becomes more apparent within the range of 0.5–2 s; within the same period range, when $\gamma < 0$, $\alpha > 1$, and the maximum value of 1.12 is obtained. (2) Opposite to the condition shown in the range of 0–2 s, during the period range of 2–5 s, with the increase of γ, α displays an increasing trend, and this trend is more evident for

Table 3: The ground "A" records for SSS (20 pairs).

Stations	Earthquakes	Components	Stations	Earthquakes	Components
5057 EI CentroArray #3	Imperial Valley (79/10/15,M6.5)	H-E03140	CHY0002	Chi-Chi (99/09/20,M7.6)	CHY002-E
		H-E03140			CHY002-N
1002 APEEL 2-Redwood City	Loma Prieta (89/10/18,M6.9)	A02043	CHY008	Chi-Chi (99/09/20,M7.6)	CHY008-E
		A02133			CHY008-N
9001 Montebeel-BR	Loma Prieta (89/10/18,M6.9)	BLF206	CHY025	Chi-Chi (99/09/20,M7.6)	CHY025-N
		BLF296			CHY008-W
58117 Treasure Island	Loma Prieta (89/10/18,M6.9)	TRI000	CHY039	Chi-Chi (99/09/20,M7.6)	CHY039-N
		TRI090			CHY039_W
0 Shin-Osaka	Kobe (95/01/16,M6.9)	SHI000	CHY041	Chi-Chi (99/09/20,M7.6)	CHY041_N
		SHI000			CHY039-W
0 Kakogawa	Kobe (95/01/16,M6.9)	KAK000	CHY092	Chi-Chi (99/09/20,M7.6)	CHY092-N
		KAK000			CHY092-W
Ambaril	Kocaeli (999/08/17,M7.4)	ATS000	CHY107	Chi-Chi (99/09/20,M7.6)	CHY0107-N
		ATS090			CHY107_W
TCU117	Chi-Chi (99/9/20,M7.6)	TCU117-N	TCU040	Landers (92/06/28,M7.3)	TCU040-N
		TCU117-W			TCU040-W
TCU118	Chi-Chi (99/09/20,M7.6)	TCU118-N	TCU111	Loma Prieta (989/10/18,M6.9)	TCU111-N
		TCU118-W			TCU111-W
CHY104	Chi-Chi (99/9/20,M7.6)	CHY104-E	TCU115	Chi-Chi (99/09/20,M7.6)	TCU115-N
		CHY104-N			TCU115-W

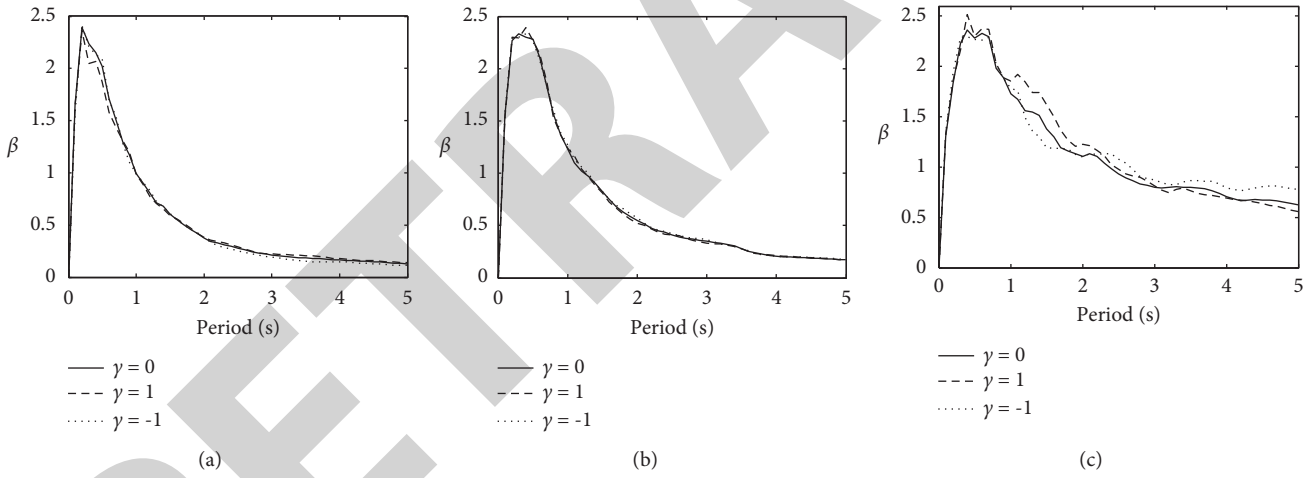

Figure 3: Amplification coefficient spectra under original one-directional earthquake "A"s ($\gamma = 0$) and superposition of bidirectional earthquake "A"s ($\gamma = 1$ and -1) (damping ratio $\xi = 0.05$). (a) Hard soil site. (b) Intermediate hard (soft) soil site. (c) Soft soil site.

the case that the ductility factor is larger and the period is longer. In this period range, when $\gamma < 0$, $\alpha < 1$, and when $\gamma > 0$, $\alpha > 1$, showing a maximum value of 1.25. Moreover, when $|\gamma|$ is around 0.6, the α curve shows peak values in the positive and negative axes, respectively; when $|\gamma| > 0.6$, the α curve displays horizontal or decreasing distribution; when $|\gamma| < 0.6$, the α curve demonstrates an almost linear increasing distribution.

Figure 7 shows the curves of α of constant ductility factors for ISS. From this figure, it is clear that, in the period range of 0–5 s, for the case that $\gamma < 0$, with the decrease of the ductility factor, α shows a tendency to increase under normal conditions, and the maximum value of α reaches 1.18, its minimum is 0.84; for the case that $\gamma > 0$, the value α mostly stays below 1, and normally, if the ductility factor is smaller, α also becomes smaller.

Figure 8 displays the curves of α of constant ductility factors for SSS. This figure illustrates the following. (1) During the period range of 0–2 s, the distribution of α along γ shows a concave shape; namely, values of α are relatively large on the two sides but relatively small in the middle of this figure, and compared to the left side, values of α on the right side are larger. However, one special condition is found within the range of 1–2 s: the α curve with a ductility factor of $\mu = 2$ shows a gradually increasing trend. (2) Compared to the distribution characteristics shown in the range of 0–2 s, during the period range of 2–5 s, α decreases with the increase of period and later remains relatively constant on the right side, and the minimum of α is around 0.9. On the left side of the figure, the value of α increases with the period, and its maximum value is close to 1.6. All of these

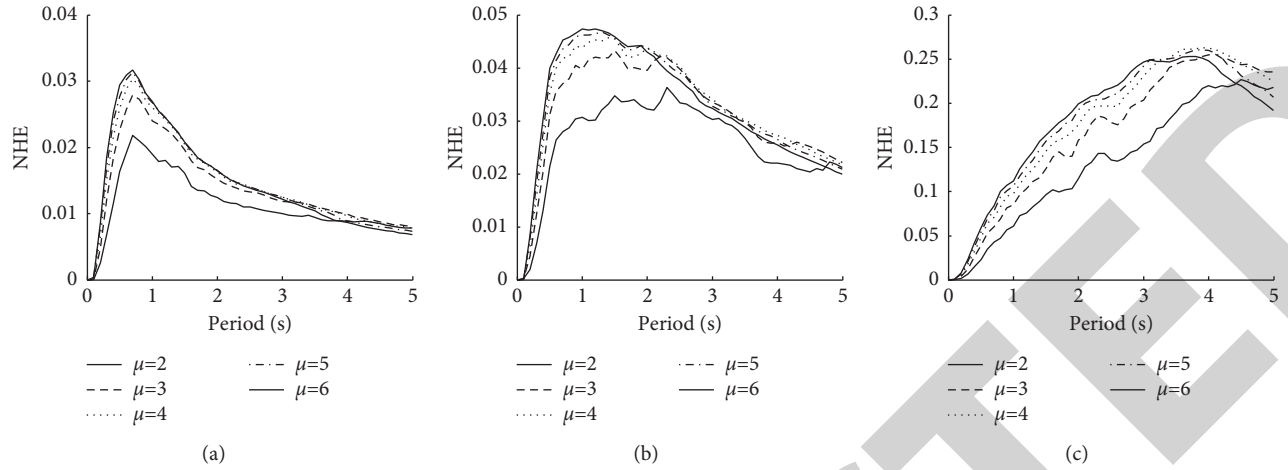

Figure 4: NHE spectra of constant ductility factors ($\gamma = 0$ and $\xi = 0.05$). (a) Hard soil site. (b) Intermediate hard (soft) soil site. (c) Soft soil site.

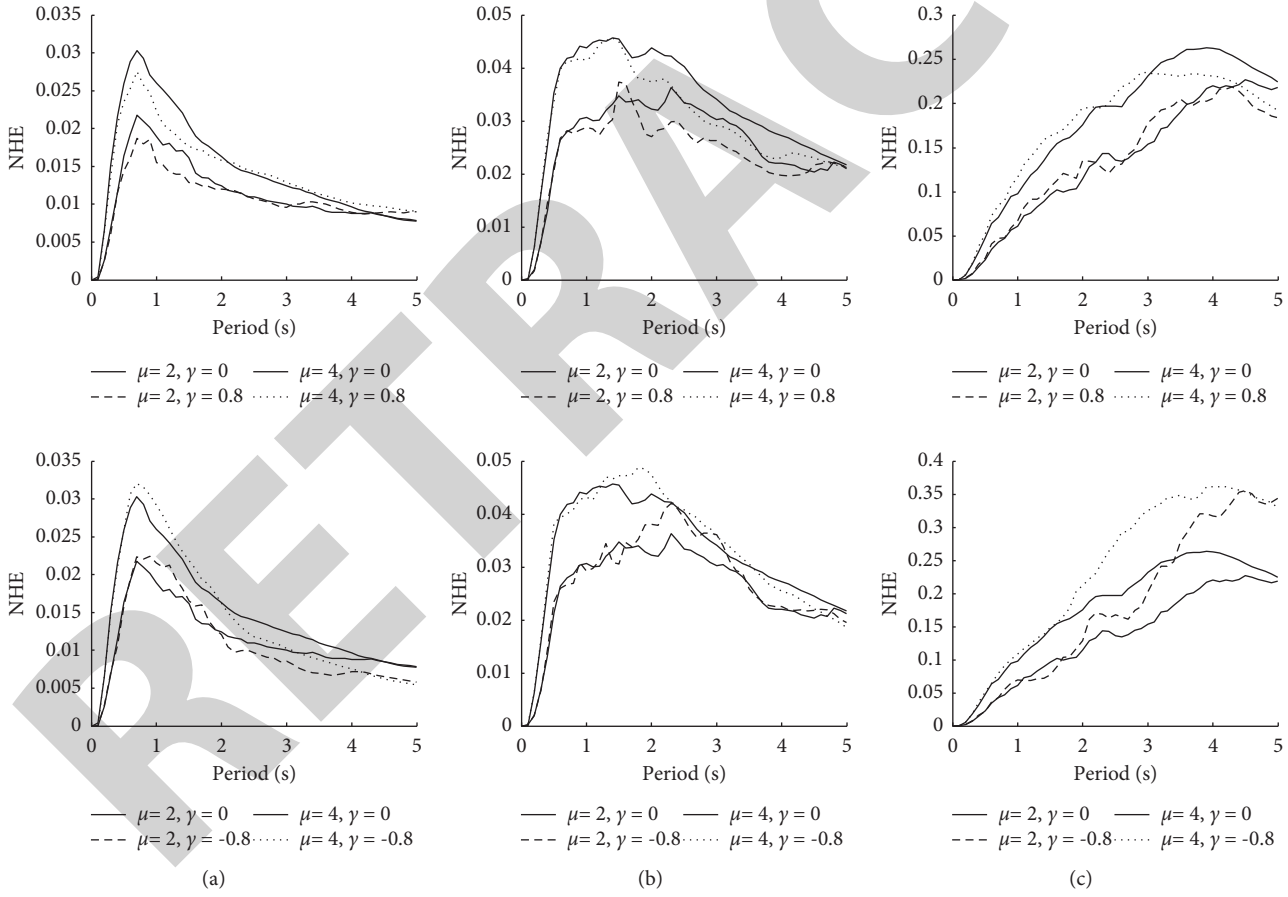

Figure 5: Comparison of NHE spectra between original one-directional GMs ($\gamma = 0$) and superposition of bidirectional GMs ($\gamma = 0.8$and -0.8) ($\xi = 0.05$). (a) Hard soil site. (b) Intermediate hard (soft) soil site. (c) Soft soil site.

distribution characteristics are easier to recognize when the ductility factor becomes smaller.

Based on the above analyses, correction coefficient α_s for correcting HE demand of conventional method is listed in Table 4. According to the approach proposed in this paper, once the HE calculated via the conventional method is multiplied by α_s, the HE demand under superposition of bidirectional GMs can be obtained. For giving the correction coefficient, the values of α_s in each period range are divided into four or three cases, for example, α_s $(-1 \le \gamma < -0.4)$, α_s $(-0.4 \le \gamma < 0)$, and α_s $(0 < \gamma \le 1)$ for the intermediate hard (soft) soil site. Regarding various γ and ductility factors μ, the values of α_s are determined

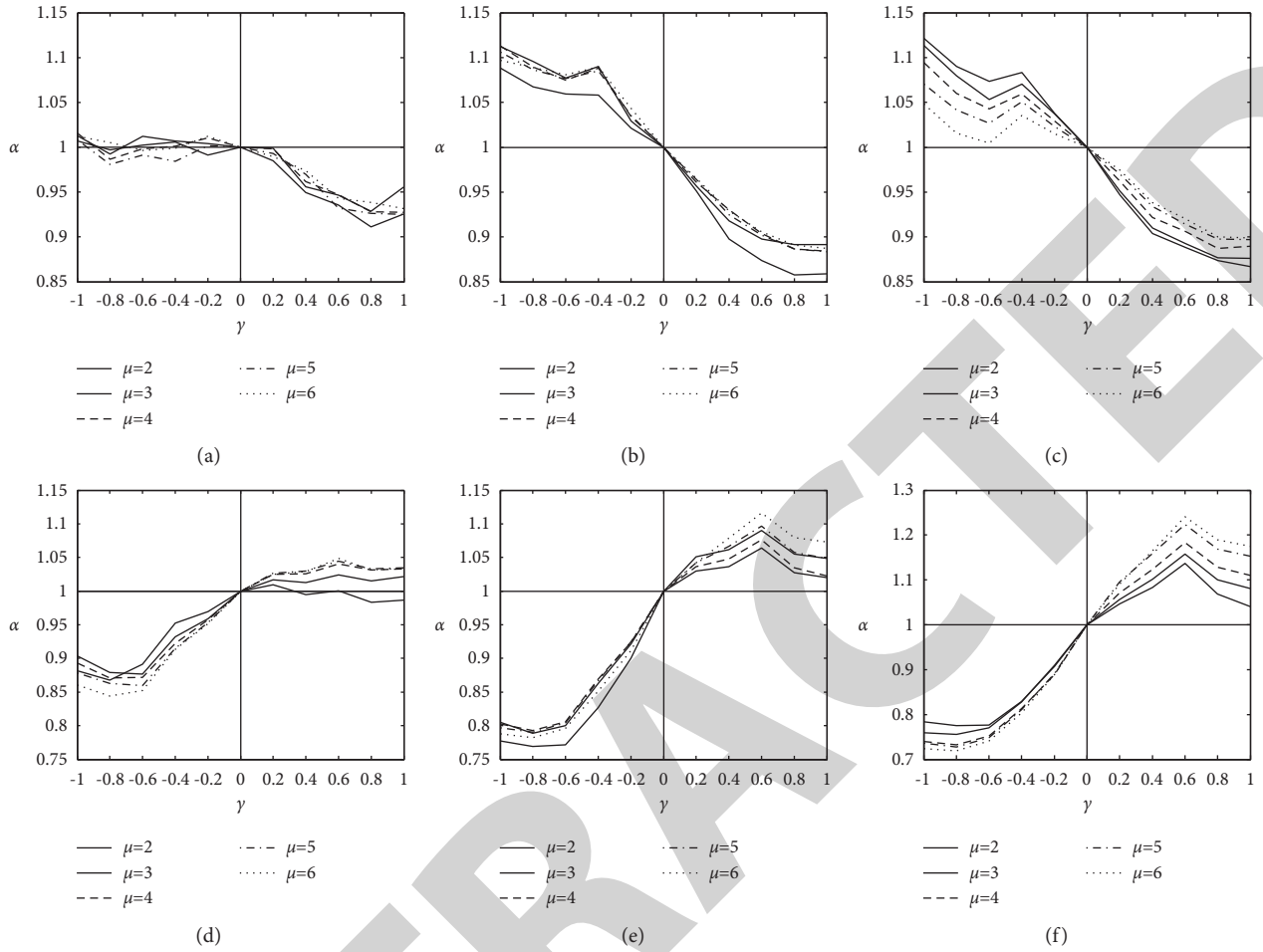

Figure 6: The curves of α of constant ductility factors for hard soil site. (a) $T = 0$–0.5 s. (b) $T = 0.5$–1.0 s. (c) $T = 1.0$–2.0 s. (d) $T = 2.0$–3.0 s. (e) $T = 3.0$–4.0 s. (f) $T = 4.0$–5.0 s.

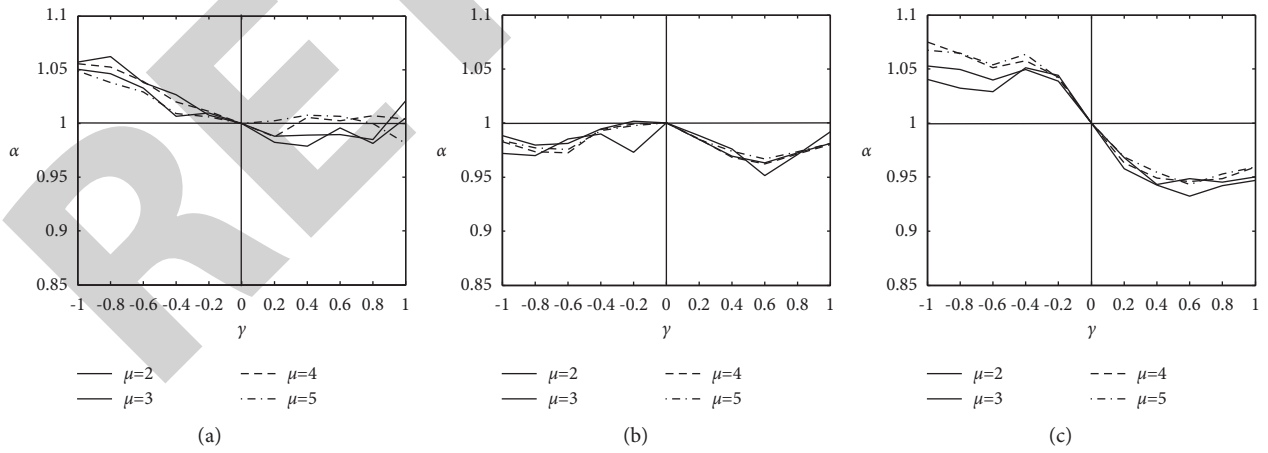

Figure 7: Continued.

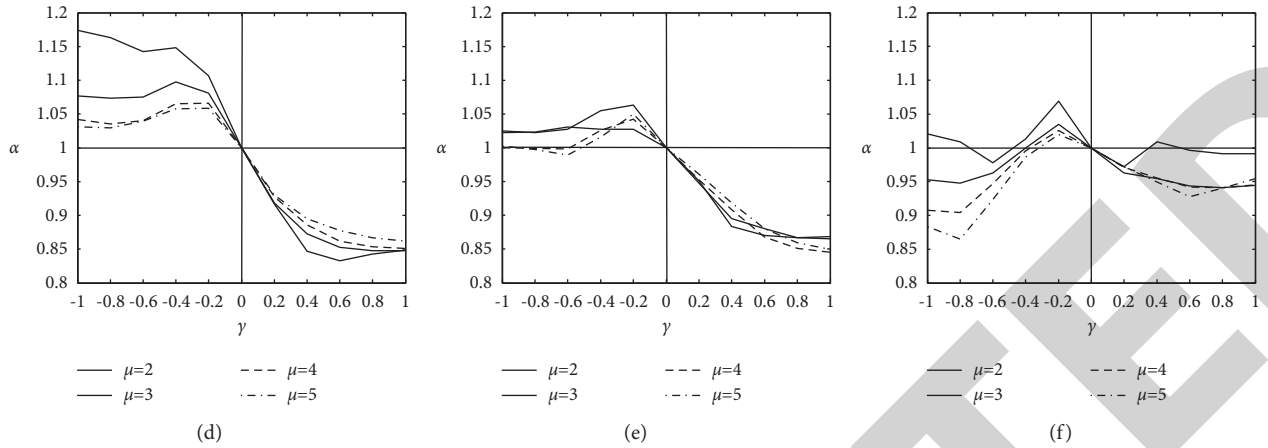

Figure 7: The curves of α of constant ductility factors for intermediate hard (soft) soil site. (a) $T = 0$–0.5 s. (b) $T = 0.5$–1.0 s. (c) $T = 1.0$–2.0 s. (d) $T = 2.0$–3.0 s. (e) $T = 3.0$–4.0 s. (f) $T = 4.0$–5.0 s.

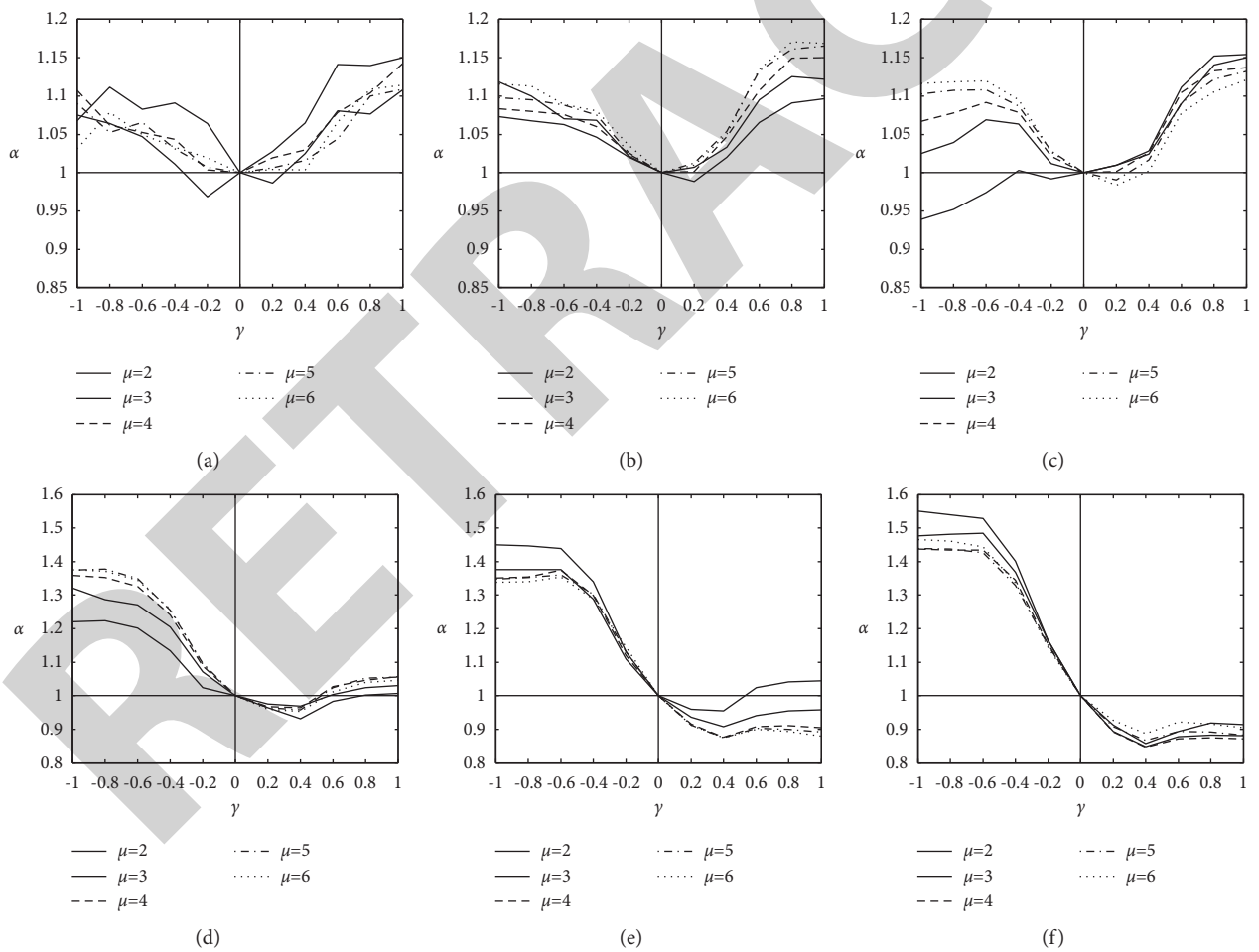

Figure 8: The curves of α of constant ductility factors for soft soil site. (a) $T = 0$–0.5 s. (b) $T = 0.5$–1.0 s. (c) $T = 1.0$–2.0 s. (d) $T = 2.0$–3.0 s. (e) $T = 3.0$–4.0 s. (f) $T = 4.0$–5.0 s.

which are the maximum values of α for each case of each period range. In this paper, only the enlargement effect of superposition of bidirectional GMs on HE demand is considered. In addition, as a consequence, if all of the α values in a certain zone are smaller than 1; $\alpha_s = 1$ should be adopted for the security reason.

Table 4: Correction coefficient α_s.

Soil site types	γ	$T = 0$–0.5 s	$T = 0.5$–1 s	$T = 1$–2 s	$T = 2$–3 s	$T = 3$–4 s	$T = 4$–5 s
HSS	$-1 \le \gamma < -0.4$	1.00	1.12	1.12	1.00	1.00	1.00
	$-0.4 \le \gamma < 0$	1.00	$-0.3\gamma + 1$	$-0.3\gamma + 1$	1.00	1.00	1.00
	$0 < \gamma \le 0.6$	1.00	1.00	1.00	$0.1\gamma + 1$	$0.2\gamma + 1$	$0.4\gamma + 1$
	$0.6 < \gamma \le 1$	1.00	1.00	1.00	1.06	1.12	1.24
ISS	$-1 \le \gamma < -0.4$	1.06	1.00	1.08	1.18	1.00	100
	$-0.4 \le \gamma < 0$	1.00	1.00	$-0.2\gamma + 1$	$-0.45\gamma + 1$	1.06	1.06
	$0 < \gamma \le 1$	1.00	1.00	1.00	1.00	1.00	1.00
SSS	$-1 \le \gamma < -0.6$	1.12	1.12	1.12	1.39	1.45	1.55
	$-0.6 \le \gamma < 0$	$-0.2\gamma + 1$	$-0.2\gamma + 1$	$-0.2\gamma + 1$	$-0.65\gamma + 1$	$-0.75\gamma + 1$	$-0.92\gamma + 1$
	$0 < \gamma \le 0.7$	$0.21\gamma + 1$	$0.24\gamma + 1$	$0.21\gamma + 1$	1.00	1.00	1.00
	$0.7 < \gamma \le 1$	1.15	1.17	1.15	1.06	1.05	1.00

5. Conclusions

Considering the irrationality of the equivalent SDOF system of a structure subjected to bidirectional GMs. The superposition of bidirectional GMs is regarded as the one-directional excitation of the equivalent SDOF system of a structure. An energy balance equation is established based on this system, and the process to determine normalized HE demand is proposed. Since the conventional theory of HE spectrum is rather mature, the ratio between NHE ($\gamma \neq 0$) and NHE ($\gamma = 0$) is analyzed to study the influence of superposition of bidirectional ground motions on HE demand. As a consequence, $\alpha_1 = \text{NHE}\ (\gamma \neq 0)/\text{NHE}\ (\gamma = 0)$ is defined, and α is defined as the mean value of α_1 in each period range. γ is set as the horizontal coordinate and α is set as the vertical coordinate, and then, the curves of α of constant ductility factors for soil types at different sites in different period ranges are established. Strong GM records are selected for establishing superimposed excitations to study the influences of soil site types, ductility factor, γ, and period on values of α. The following conclusions are achieved through analysis:

(i) For the HSS, during the period range of 0–2 s, α increases with the decrease of γ; especially, for the case that the ductility factor is smaller and the period is longer, this decrease trend is more apparent. Within the same period range (0–2 s), when $\gamma < 0$, $\alpha > 1$, and when $\gamma > 0$, $\alpha < 1$. During the period range of 2–5 s, α increases with the increase of γ; especially, for the case that the ductility factor becomes larger and the period is longer, this increase trend is more evident. Within the same period range (2–5 s), when $\gamma < 0$, $\alpha < 1$, and when $\gamma > 0$, $\alpha > 1$.

(ii) For the ISS, during the period range of 0–5 s, for $\gamma < 0$, normally the smaller the ductility factor, the larger the value of α, and with the increase of the period, the value of α first increases and then decreases. For $\gamma > 0$, normally, the smaller the ductility factor, the smaller the value of α, and the value of α first decreases and then increases with the increase of the period.

(iii) For the SSS, during the period range of 0–2 s, the distribution of α along γ shows an approximate concave shape, and normally, $\alpha > 1$. Within the period range of 2–5 s, the distributions of α on both sides of the curves are almost horizontal; the values of α are lower with the increase of γ in the middle of the curves. In the same range (2–5 s), when $\gamma < 0$, $\alpha > 1$, and α increases with the increase of the period. This characteristic becomes more apparent with a smaller ductility factor.

Based on the analysis concerning distribution characteristics of α along with γ, the correction coefficient for easier application, namely, α_s, is given, which is the simplified value of α. The value of α_s, combined with conventional HE spectrum, can be used to determine HE demand corresponding to the different γ, and then, the HE demand of the structure subjected to bidirectional GMs can be estimated.

Data Availability

All the data can be obtained from the corresponding author upon request.

Conflicts of Interest

The authors declare that they have no conflicts of interest.

Acknowledgments

This study was supported by the National Natural Science Foundation of China (no. 51478091) and the Young and Middle-aged Talents research Project of the National Ethnic Affairs Commission of China in 2019 (no. 0908210012).

References

[1] I. Iervolino, G. Maddaloni, and E. Cosenza, "Eurocode 8 compliant real record sets for seismic analysis of structures," *Journal of Earthquake Engineering*, vol. 12, no. 1, pp. 54–90, 2008.

[2] I. Iervolino, C. Galasso, and E. Cosenza, "REXEL: computer aided record selection for code-based seismic structural analysis," *Bulletin of Earthquake Engineering*, vol. 8, no. 2, pp. 339–362, 2010.

[3] M. D. Trifunac, "Biot response spectrum," *Soil Dynamics and Earthquake Engineering*, vol. 26, no. 6-7, pp. 491–500, 2006.

[4] M. D. Trifunac, "Earthquake response spectra for performance based design-a critical review," *Soil Dynamics and Earthquake Engineering*, vol. 37, pp. 73–83, 2012.

[5] J. J. Bommer, M. Papaspiliou, and W. Price, "Earthquake response spectra for seismic design of nuclear power plants in the UK," *Nuclear Engineering and Design*, vol. 241, no. 3, pp. 968–977, 2011.

[6] A. K. Chopra, "Elastic response spectrum: a historical note," *Earthquake Engineering & Structural Dynamics*, vol. 36, no. 1, pp. 3–12, 2007.

[7] J. P. Wolf, *Dynamic Soil-Structure Interaction*, Prentice-Hall, Englewood Cliffs, NJ, USA, 1985.

[8] M. Čaušević and E. Zehentner, "Nonlinear seismic calculation of structures according to EN 1998-1: 2004," *Građevinar*, vol. 59, no. 9, pp. 767–777, 2007.

[9] A. Benavent-Climent, "An energy-based method for seismic retrofit of existing frames using hysteretic dampers," *Soil Dynamics and Earthquake Engineering*, vol. 31, no. 10, pp. 1385–1396, 2011.

[10] G. Ghodrati Amiri, G. A. Darzi, and J. Vaseghi Amiri, "Design elastic input energy spectra based on Iranian earthquakes," *Canadian Journal of Civil Engineering*, vol. 35, no. 6, pp. 635–646, 2008.

[11] A. Habibi, R. W. K. Chan, and F. Albermani, "Energy-based design method for seismic retrofitting with passive energy dissipation systems," *Engineering Structures*, vol. 46, pp. 77–86, 2013.

[12] F. Wang, N. Zhang, and Z. Y. Huang, "Estimation of earthquake induced story hysteretic energy of multi-story buildings," *Earthquakes and Structures*, vol. 11, no. 1, pp. 165–178, 2016.

[13] Y. Q. Zhang, J. Chen, and C. X. Sun, "Damage-based strength reduction factor for nonlinear structures subjected to sequence-type ground motions," *Soil Dynamics and Earthquake Engineering*, vol. 92, pp. 298–311, 2017.

[14] R. Greco, G. C. Marano, and A. Fiore, "Damage-based inelastic seismic spectra," *World Scientific*, vol. 17, no. 10, Article ID 1750115, 2017.

[15] Y. Li, X. Z. Lu, H. Guan, and L. P. Ye, "An energy-based assessment on dynamic amplification factor for linear static analysis in progressive collapse design of ductile RC frame structures," *Advances in Structural Engineering*, vol. 17, no. 8, pp. 1217–1225, 2014.

[16] S. Leelataviwat and S. C. Goel, "Energy-based seismic design of structures using yield mechanism and target drift," *Journal of Structural Engineering*, vol. 128, no. 8, pp. 1046–1054, 2002.

[17] M. Bruneau and N. Wang, "Normalized energy-based methods to predict the seismic ductile response of SDOF structures," *Engineering Structures*, vol. 18, no. 1, pp. 13–28, 1996.

[18] L. D. Decanini and F. Mollaioli, "An energy-based methodology for the seismic assessment of seismic demand," *Soil Dynamics and Earthquake Engineering*, vol. 21, pp. 113–137, 2001.

[19] E. Erduran, "Hysteretic energy demands in multi-degree-of-freedom systems subjected to earthquakes," *Buildings*, vol. 10, no. 220, pp. 1–17, 2020.

[20] A. Benavent-Climent, F. Lopez-Almanse, and D. A. Bravo-Gonzalez, "Design energy input spectra for moderate-to-high seismicity regions based on Colombian earthquakes," *Soil Dynamics and Earthquake Engineering*, vol. 30, pp. 1129–1148, 2010.

[21] D. Arroyo and M. Ordaz, "On the estimation of hysteretic energy demands for SDOF systems," *Earthquake Engineering & Structural Dynamics*, vol. 36, pp. 2365–2382, 2007.

[22] R. Riddell and J. E. Garcia, "Hysteretic energy spectrum and damage control," *Earthquake Engineering & Structural Dynamics*, vol. 30, pp. 1791–1816, 2001.

[23] C. C. Chou and C. M. Uang, "Establishing absorbed energy spectra—an attenuation approach," *Earthquake Engineering & Structural Dynamics*, vol. 29, pp. 1441–1455, 2000.

[24] Y. Hagiwara, "Momentary energy absorption and effective loading cycles of structures during earthquakes," in *Proceedings of the 15th World Conference on Earthquake Engineering*, Auckland, New Zealand, January 2000.

[25] S. K. Kunnanth and H. Chai, "Cumulative damage-based inelastic cyclic demand spectrum," *Earthquake Engineering & Structural Dynamics*, vol. 33, pp. 499–520, 2004.

[26] F. Wang and H. N. Li, "Energy spectra of constant ductility factors for orthogonal bidirectional earthquake excitations," *Advances in Structural Engineering*, vol. 18, no. 11, pp. 1887–1899, 2015.

[27] J. C. Reyes and A. K. Chopra, "Three-dimensional modal pushover analysis of buildings subjected to two components of ground motion, including its evaluation for tall buildings," *Earthquake Engineering & Structural Dynamics*, vol. 40, pp. 789–806, 2011.

[28] Z. W. Miao, L. P. Ye, H. Guan, and X. Z. Lu, "Evaluation of modal and traditional pushover analyses in frame-shear-wall structures," *Advances in Structural Engineering*, vol. 14, no. 5, pp. 815–836, 2011.

[29] G. Manoukas, A. Athanatopoulou, and L. Avramidis, "Multimode pushover analysis for asymmetric buildings under biaxial seismic excitation based on a new concept of the equivalent single degree of freedom system," *Soil Dynamics and Earthquake Engineering*, vol. 38, pp. 88–96, 2012.